ELSEVIER

Journal of Structural Geology 26 (2004) 2089–2102

JOURNAL OF STRUCTURAL GEOLOGY

www.elsevier.com/locate/jsg

Crystal preferred orientations of garnet: comparison between numerical simulations and electron back-scattered diffraction (EBSD) measurements in naturally deformed eclogites

David Mainprice[a,*], Jérôme Bascou[a], Patrick Cordier[b], Andréa Tommasi[a]

[a]*Laboratoire de Tectonophysique, CNRS & Université Montpellier II, France*
[b]*Laboratoire de Structure et Propriétés de l'Etat Solide, CNRS & Université Lille I, France*

Received 26 March 2003; received in revised form 8 April 2004; accepted 24 April 2004

Available online 10 July 2004

Abstract

Observations of dislocations, sub-grains and elongated crystal shapes support plastic deformation of garnet in laboratory experiments and naturally deformed eclogites. To evaluate the crystal preferred orientations (CPO) of garnet formed in axial shortening, pure shear and simple shear, we performed numerical simulations of CPO development during plastic flow using the visco-plastic self-consistent model. As input for the models we use the slip systems determined by transmission electron microscopy using experimentally deformed specimens. Although in garnet 66 slip systems are available, slip on the ⟨111⟩{110} system provides over 86% of the total strain in the simulations. Characteristic CPO distributions are produced for the three deformation paths, with the CPO being strongest for axial shortening and weakest for simple shear. Compared with low-symmetry minerals, the pole figure densities of garnet, which has cubic symmetry, are weak. ⟨100⟩ axes tend to align with the shortening direction in all three deformation modes. The simulations are compared with CPO of naturally deformed garnet from nine eclogite samples from the Alps, Norway, and Mali, which contain 20–40% garnet. All samples show weak garnet CPO. Only two samples have a CPO pattern similar to the simulations for simple shear, no samples are similar to simulations for axial strain or pure shear. The presence of other weaker minerals, such as omphacite and quartz, with volume fractions higher than garnet, probably prevented garnet from becoming highly strained and developing characteristic CPOs in these eclogites. Higher volume fractions of garnet and higher temperature conditions may, however, allow the development of garnet CPO in the mantle transition zone, particularly within subducted oceanic material (MORB).

Keywords: Crystal preferred orientation; Deformation; Dislocation glide; Eclogites; Subduction

1. Introduction

In recent years there has been a growing interest in the plasticity of garnet, since it is an important component that may significantly affect the deformation of the lower continental crust, of ultra-high pressure rocks associated with subduction, such as eclogites, and of the upper mantle (below 70 km). Moreover, in the mid-mantle, garnet is a volumetrically important mineral; in the transition zone (410–670 km depth), a pyrolite mantle and subducted oceanic crust contain up to 40 and 90% of garnet, respectively. In the past, the isotropic optical properties of garnet have hindered the study of its internal deformation features and crystallographic orientations. Some early studies by Dalziel and Bailey (1968), Carstens (1969, 1971), and Ross (1973) suggested, however, that garnet deforms plastically. More recently, there has been some controversy about the importance of garnet plasticity in various geological settings and the possible role of solution–precipitation in the ductility of garnets (Ji and Martignole, 1994; Den Brok and Kruhl, 1996; Ji and Martignole, 1996; Ji et al., 2003). Prior et al. (2000, 2002) and Kleinschodt and McGrew (2000) have imaged sub-grains in naturally deformed garnets using SEM-based techniques, which they interpret as an indicator of plastic deformation. Kleinschodt and McGrew (2000) have also measured the crystal preferred orientation (CPO) of garnet using electron-channelling patterns (ECP) and shown that

* Corresponding author. Tel.: +33-04-67-14-36-02; fax: +33-04-67-14-36-03.
E-mail address: david@dstu.univ-montp2.fr (D. Mainprice).

0191-8141/$ - see front matter © 2004 Published by Elsevier Ltd.
doi:10.1016/j.jsg.2004.04.008

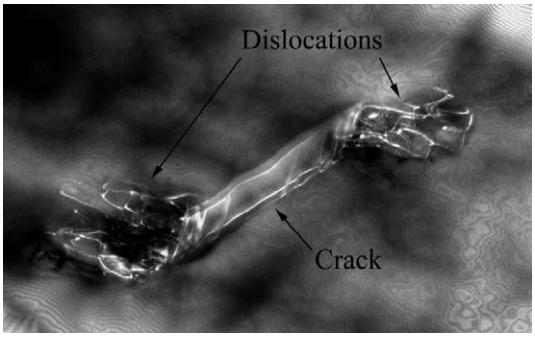

Fig. 1. Pyrope–Almandine garnet deformed experimentally in a multianvil apparatus at 900 °C, 6 GPa (Voegelé, 1998). Dislocation loops emitted at a microcrack tip. Weak-beam dark-field TEM micrograph, $\mathbf{g} = (400)$. Courtesy of V. Voegelé.

there is a degree of preferred orientation. Finally, transmission electron microscope (TEM) studies of dislocations in naturally deformed garnet (Ando et al., 1993; Doukhan et al., 1994; Voegelé et al., 1998; Ji et al., 2003) showed that dislocation slip occurs.

This study aims to answer the question: 'does deformation of garnet by dislocation glide result in a characteristic CPO?' To reach that objective, we firstly briefly review the evidence for dislocation plasticity and data on the active slip systems from high-temperature experimental deformation. Secondly, we present a series of VPSC models of CPO development based on the observed slip systems for a series of finite strain paths. Thirdly, we present the CPO of naturally deformed garnet for a series of high-pressure eclogites measured using electron back-scattered diffraction (EBSD) and compare these with our simulations.

2. Deformation mechanisms in garnets

The structure of garnets is based on a bcc lattice (space group Ia3d). Deformation experiments performed on

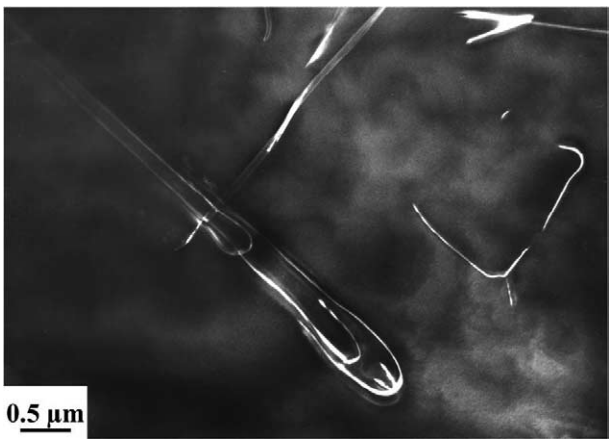

Fig. 2. Pyrope–Almandine garnet deformed experimentally in a multianvil apparatus at 900 °C, 6 GPa (Voegelé, 1998). Gliding dislocation loops with a Burger vector [100]. Weak-beam dark-field TEM micrograph, $\mathbf{g} = (400)$. Courtesy of V. Voegelé.

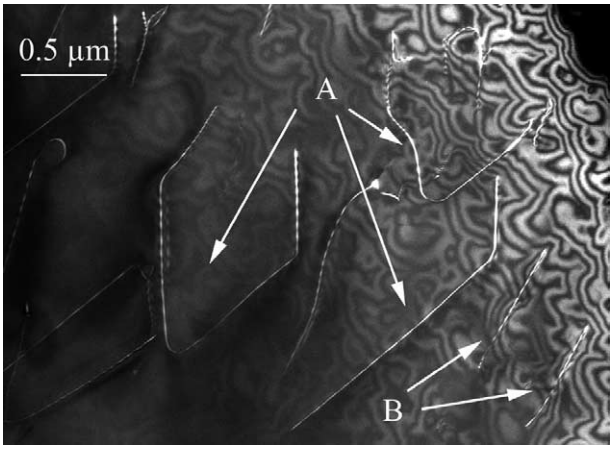

Fig. 3. Pyrope–Almandine garnet deformed experimentally in a multianvil apparatus at 1100 °C, 6 GPa (Voegelé, 1998). Gliding dislocation loops. (A) $1/2[1\bar{1}1]$ dislocations gliding in (101); (B) $1/2[1\bar{1}1]$ dislocations gliding in $(3\bar{1}\bar{2})$. Weak-beam dark-field TEM micrograph, $\mathbf{g} = (400)$. Courtesy of V. Voegelé.

synthetic garnets YAG (Hardiman et al., 1972; Parthasarathy et al., 1992; Corman, 1993; Karato et al., 1994; Blumenthal and Phillips, 1996), YIG (Rabier et al., 1976a,b, 1979, 1981; Rabier, 1979), GGG (Garem et al., 1982, 1985; Garem, 1983; Wang et al., 1996) and CGGG (Voegelé et al., 1999) have shown that the dislocation structures in garnets can be, to a first approximation, compared with those in bcc metals. The shortest lattice repeat is $1/2\langle 111\rangle$ and one can expect plastic deformation to be dominated by $1/2\langle 111\rangle$ dislocations. $1/2\langle 111\rangle$ dislocations from different slip systems are likely to react and form junctions following the reaction: $1/2[1\bar{1}1] + 1/2[11\bar{1}] \rightarrow [100]$.

Several studies have provided evidence for plastic deformation of garnets in naturally deformed rocks (Dalziel and Bailey, 1968; Carstens, 1969, 1971; Ross, 1973; Allen et al., 1987; Ando et al., 1993; Doukhan et al., 1994; Ji and Martignole, 1994; Chen et al., 1996; Voegelé et al., 1998b; Kleinschodt and McGrew, 2000; Prior et al., 2000). Experimental deformation of silicate garnets has also been carried out by several groups (Ingrin and Madon, 1995; Karato et al., 1995; Cordier et al., 1996; Voegelé et al., 1998a; Wang and Ji, 1999). Experiments as well as studies of natural materials suggest that garnets undergo a brittle–ductile transition that, in nature, occurs at about 600–800 °C (Voegelé et al., 1998b; Wang and Ji, 1999).

In the low-temperature, brittle regime, garnet grains appear to be rigid macroscopically. Crystal plasticity, if it occurs, is restricted to the vicinity of cracks (Fig. 1). Dislocations are nucleated due to stress concentration at the crack tips, but they do not expand very far from the tip. Beyond the usual $1/2\langle 111\rangle$ and $\langle 100\rangle$ dislocations, one also finds dislocations with unusually large Burgers vectors such as $\langle 110\rangle$. These dislocations often exhibit dissociation.

Above the brittle–ductile transition, garnets deform by dislocation creep. TEM characterization of experimentally deformed specimens has shown that glide of $\langle 100\rangle$

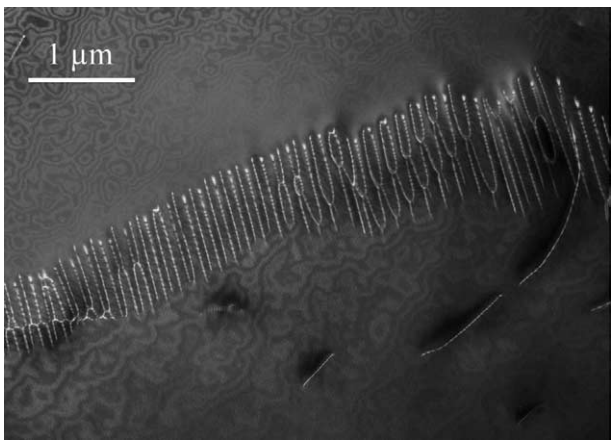

Fig. 4. Subgrain boundary in a garnet grain from a garnet pyroxenite (Lherz). Sample 70.291 kindly provided by V. Sautter. Weak-beam dark-field TEM micrograph, $\mathbf{g} = (400)$. Courtesy of V. Voegelé.

dislocations in {011} and {010} planes (Fig. 2) contribute significantly to plastic deformation (Voegelé et al., 1998a). Using large-angle convergent beam electron diffraction (LACBED) measurements, Voegelé et al. (1998b) have also observed $1/2\langle 111\rangle$ dislocations that glide in three families of planes: {110}, {112} and {123}. Although {110} is the most frequently observed plane, glide on these three families of planes seems to be equally easy (Fig. 3). Dislocations in garnet often exhibit very marked crystallographic orientations characteristic of a large lattice friction (Fig. 3). In addition to evidence for deformation by dislocation glide at high temperature, many studies have emphasized the occurrence of well-organized sub-grain boundaries (Fig. 4), which indicates that climb and recovery accompany dislocation glide (Carstens, 1969; Ando et al., 1993; Doukhan et al., 1994; Ji and Martignole, 1994; Voegelé et al., 1998a,b; Wang and Ji, 1999; Kleinschodt and McGrew, 2000; Prior et al., 2000).

3. Crystal preferred orientation modelling

Garnet CPOs developed under different deformation regimes are predicted using a viscoplastic self-consistent model (VPSC) (Molinari et al., 1987), which was extended to anisotropic plasticity by Lebensohn and Tomé (1993). The pioneering work in Earth Sciences of Wenk and co-workers (e.g. Wenk et al., 1991) has established that this visco-plastic self-consistent (VPSC) model provides a robust solution, which reproduces the essential features of CPOs of experimentally deformed plastically anisotropic minerals. Recently, this model has been successfully applied to polycrystalline ice (Castelnau et al., 1996), olivine (Tommasi et al., 2000) and clinopyroxene (Bascou et al., 2002). In contrast to classical lower or upper bound approaches, that impose respectively static bound (uniform stress) or homogeneous strain (Taylor, 1938) within the aggregate, the VPSC approach allows both the microscopic stress and strain rate to differ from the corresponding macroscopic quantities. Strain compatibility and stress equilibrium are ensured only for volume-averaged tensors at the aggregate scale.

At the grain scale, deformation is accommodated by dislocation glide only; other deformation processes such as dislocation climb, grain boundary sliding or dynamic recrystallization are not specifically taken into account. The shear rate in a slip system s is related to the local deviatoric stress tensor $\mathbf{s}$ by a viscoplastic law:

$$\dot{\gamma}^s = \dot{\gamma}_0 \left(\frac{\tau_r^s}{\tau_0^s} \right)^{n^s} = \dot{\gamma}_0 \left(\frac{r_{ij}^s s_{ij}}{\tau_0^s} \right)^{n^s} \tag{1}$$

where $\dot{\gamma}_0$ is a reference strain rate, taken as 1 s^{-1}, and n^s, τ_r^s, and τ_0^s are, respectively, the stress exponent, the resolved shear stress, and the critical resolved shear stress (CRSS) for the system s, whose orientation relative to the macroscopic axes is expressed by its Schmid tensor $\mathbf{r}^s$.

The problem lies in the calculation of a microscopic state ($\mathbf{s}$, $\dot{\boldsymbol{\epsilon}}$) for each grain, whose volume average determines the response of the polycrystal ($\bar{\Sigma}$, $\bar{\mathbf{D}}$). The '1-site' approximation (Molinari et al., 1987; Lebensohn and Tomé, 1993) is used in the anisotropic VPSC formulation; the influence of neighbouring grains is not taken into account. Interactions between each grain and its surroundings are successively replaced by the interaction between an inclusion with similar lattice orientation and an infinite homogeneous equivalent medium (HEM), whose behaviour is the weighted average of the grains. This leads to:

$$\dot{\epsilon}_{ij} - D_{ij} = -\alpha \tilde{\mathbf{M}}_{ijkl} \left(s_{kl} - \bar{\Sigma}_{kl} \right) \tag{2}$$

where $\tilde{\mathbf{M}}$ is the interaction tensor and α is a constant used to parameterize the interaction between grains and the HEM. $\alpha = 0$ corresponds to the upper bound model (homogeneous strain), $\alpha = 1$ is the classical self-consistent model (a linear relationship between volume averaged stress and strain rate) and $\alpha = \infty$ corresponds to the lower bound model (stress equilibrium).

Prescribing a constant macroscopic velocity gradient tensor $\mathbf{L}$ imposes the strain history. In the present models, the velocity gradient tensors are given, respectively, by:

$$\mathbf{L} = \begin{bmatrix} 0.5 & 0 & 0 \\ 0 & -1 & 0 \\ 0 & 0 & 0.5 \end{bmatrix}, \qquad \mathbf{L} = \begin{bmatrix} 1 & 0 & 0 \\ 0 & -1 & 0 \\ 0 & 0 & 0 \end{bmatrix}$$
$$\text{and} \qquad \mathbf{L} = \begin{bmatrix} 0 & 1 & 0 \\ 0 & 0 & 0 \\ 0 & 0 & 0 \end{bmatrix} \tag{3}$$

for axial compression, pure shear, and simple shear simulations. The time increment, $d\tau$, is set to achieve an equivalent strain of 0.025 in each deformation step. The

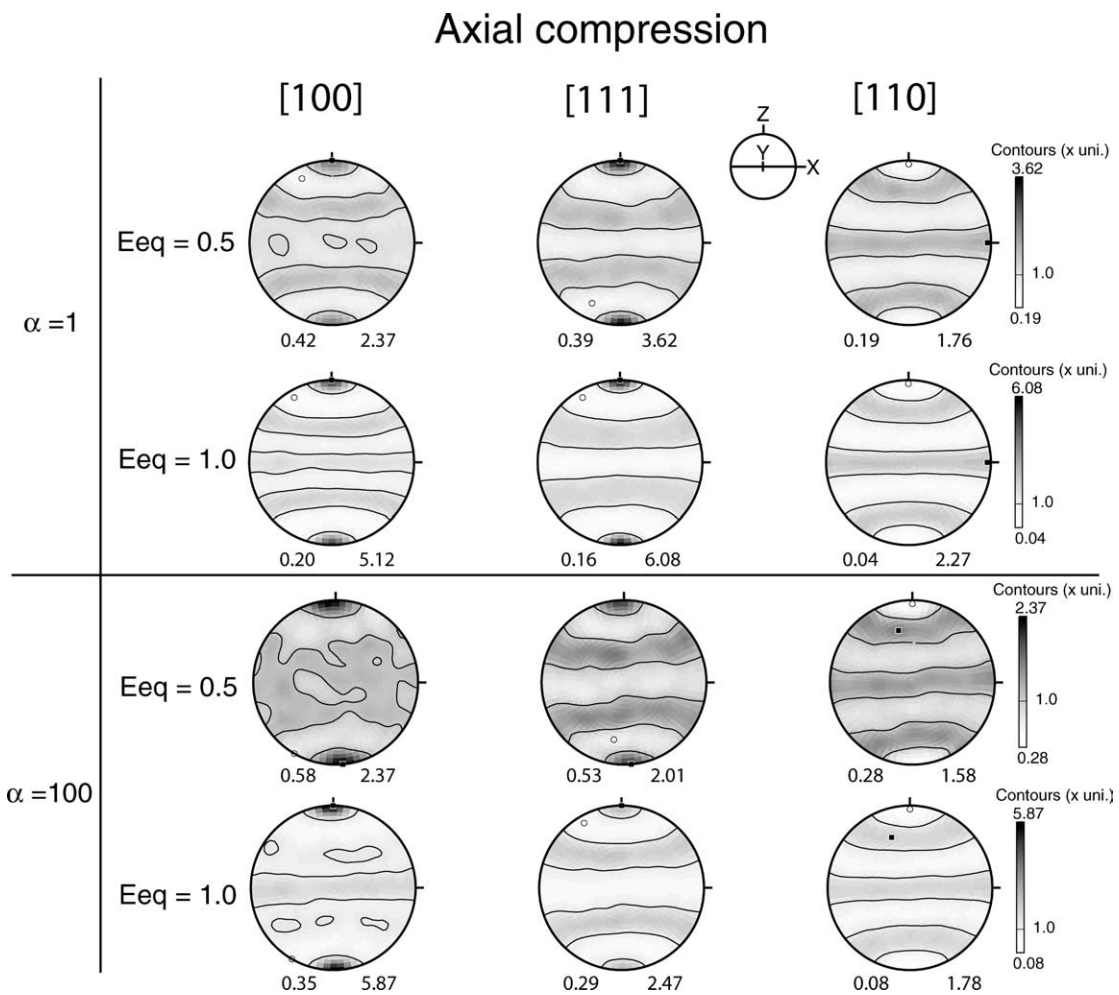

Fig. 5. Garnet [100], ⟨111⟩ and [110] pole figures for VPSC models $\alpha = 1$ and $\alpha = 100$ and equivalent strains of 0.5 and 1.0 for axial compression. Compression axis (Z) is vertical. X and Z are finite strain axes with X and Z being the direction of maximum and minimum extension directions, respectively. Lower hemisphere plots. The contour at one times multiple of a uniform distribution is plotted. An inverse log grey scale also displays densities.

equivalent strain is defined as:

$$\epsilon_{\mathrm{eq}} = \int \mathbf{D}_{\mathrm{eq}}(\tau)\mathrm{d}\tau \tag{4}$$

where the Von Mises equivalent strain rate is:

$$\mathbf{D}_{\mathrm{eq}} = \sqrt{2/3\mathbf{D}_{ij}\mathbf{D}_{ij}} \tag{5}$$

In the present simulations, a constant velocity gradient tensor was maintained for 40 identical steps of 0.025 equivalent strain giving a final equivalent strain of 1.0 (or a shear strain of $\gamma = 1.73$ for simple shear). The model aggregates are composed of 1000 randomly oriented spherical grains. The only tuning parameters are therefore the active slip systems for garnet, their critical resolved shear stresses (CRSS) and stress exponents (n) and the strength of the interaction between grains and the HEM, defined by α.

In nature, activation of non-glide mechanisms, like climb or grain boundary sliding, may contribute to relax the strain compatibility requirements. Setting the interaction parameter $? > 1$, and hence approaching the stress equilibrium model, may simulate this. TEM observations of dislocations in garnet did show evidence for dislocation climb. To evaluate the influence of relaxing the strain compatibility, we present models with $\alpha = 1$ and 100.

High-temperature experiments on garnet single crystals oriented to glide on $1/2\langle 111\rangle(1\bar{1}0)$ have a stress exponent of 3.0 ± 0.5 (Wang and Ji, 1999). Jin et al. (2001) measured a value of $n = 3.4 \pm 0.5$ on experimentally deformed synthetic eclogite containing 50% garnet. Such stress exponents imply that dislocation climb is active (Poirier, 1985). The VPSC model is not very sensitive to n between 3 and 5, increasing n only increases the degree of CPO for a given finite strain. Thus we used a value of $n = 3$ in all models.

The slip systems in garnet were determined by TEM as described above, but we do not know their CRSS. Since the density of dislocations is proportional to the internal stress raised to the power of two (Poirier, 1985), the higher density of ⟨100⟩ than $1/2\langle 111\rangle$ dislocations (Voegelé, 1998) suggests that ⟨100⟩ slip is characterized by a higher critical resolved shear stress than $1/2\langle 111\rangle$ slip. We have set the

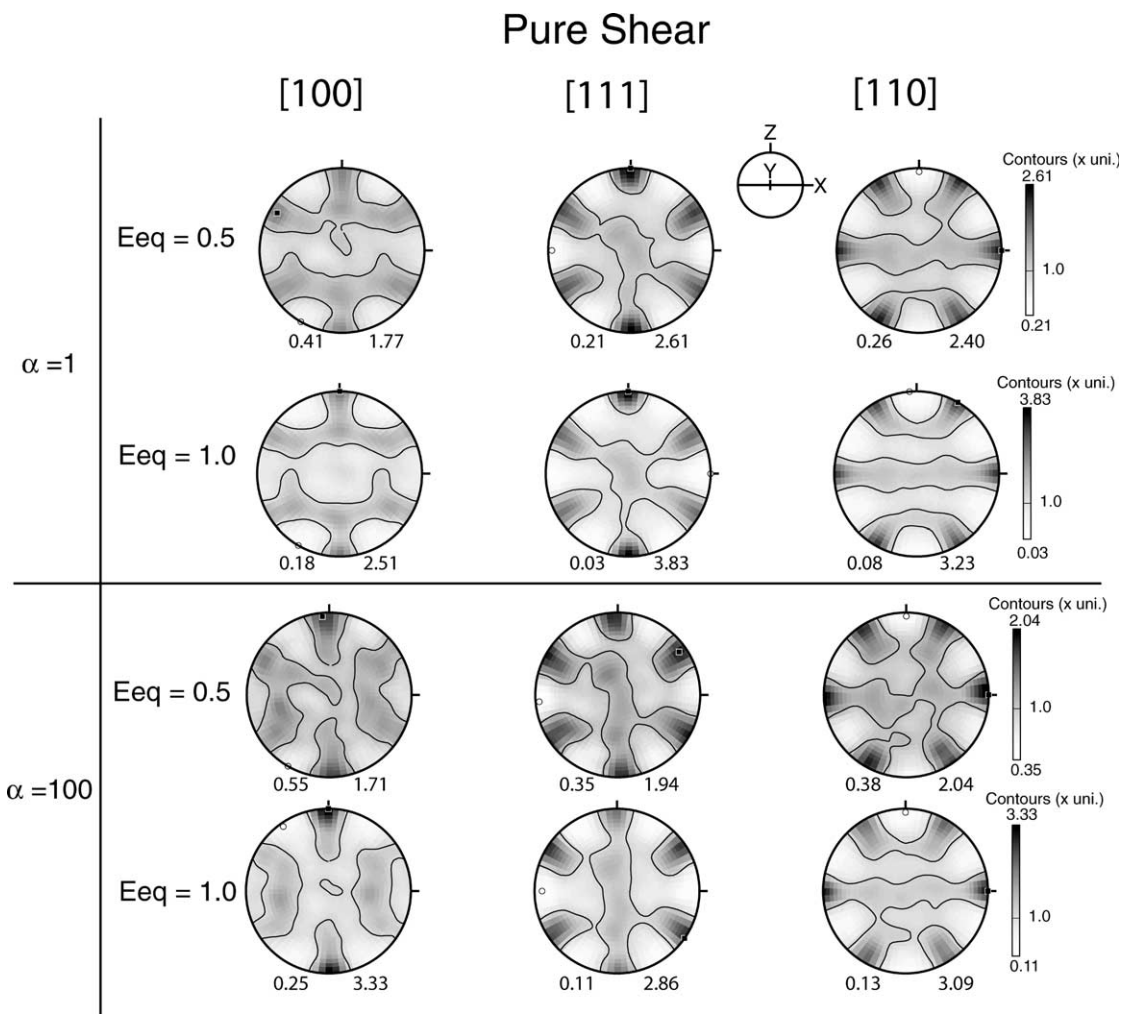

Fig. 6. Garnet [100], ⟨111⟩ and [110] pole figures for VPSC models $\alpha = 1$ and $\alpha = 100$ and equivalent strains of 0.5 and 1.0 for pure shear. Compression axis (Z) is vertical and extension axis (X) is horizontal. X and Z are finite strain axes with X and Z being the direction of maximum and minimum extension directions, respectively. Lower hemisphere plots. The contour at one times multiple of a uniform distribution is plotted. An inverse log grey scale also displays densities.

relative CRSS for1/2⟨111⟩ and ⟨100⟩ at 1 and 3, respectively, meaning that critical resolved shear stress needed to activate ⟨100⟩ is three times that of 1/2⟨111⟩. ⟨110⟩ Burgers vector is only observed at low temperature and hence high stress, so we set its CRSS to five. We note the CRSS values we have used for garnet have an approximately linear relationship to the square of the modulus of Burgers vector and to the elastic stored energy (E) for these dislocations. The chosen CRSS values thus appears to be a physically consistent choice, since E is proportional to the stress necessary to bow a straight dislocation or activate a Frank–Reid dislocation source.

Silicate garnet has similar slip systems to body centred cubic (bcc) metals for which Taylor and Elam (1926) introduced the concept of 'pencil glide' to explain the wavy nature of slip lines perpendicular to ⟨111⟩ in iron. The slip planes were assumed to be {110}, {112} and {123} or any plane with ⟨111⟩ as zone axis, which are essentially the same as those identified for silicate garnet by TEM. Potentially there are 96 different slip systems for ⟨111⟩ direction on 12 planes of types {110} and {112}, and 24 planes of type {123} as the CRSS could be different in positive and negative directions. Such a difference is observed, for instance, for slip on {112} in bcc metals where the resistance for plastic shear is smaller in the same sense as a twinning-shear $\langle \bar{1}\bar{1}1 \rangle$ than in the opposite direction $\langle 11\bar{1} \rangle$ (e.g. Hull and Bacon, 1995). Even if we assume that positive and negative directions have the same CRSS for garnet, as we have done in the present VPSC models, since we do not have any information to the contrary, then there are still 48 slip systems associated with1/2⟨111⟩ on {110}, {112} and {123} planes. To these 1/2⟨111⟩ systems we must add the six systems each for [110] {001}, [100] {010} and [100] {011}, giving a final total of 66 slip systems for garnet. Clearly there is no problem finding five independent slip systems per crystal necessary to meet the Von Mises criterion for strain compatibility at large strains.

CPO simulations for axial compression at equivalent

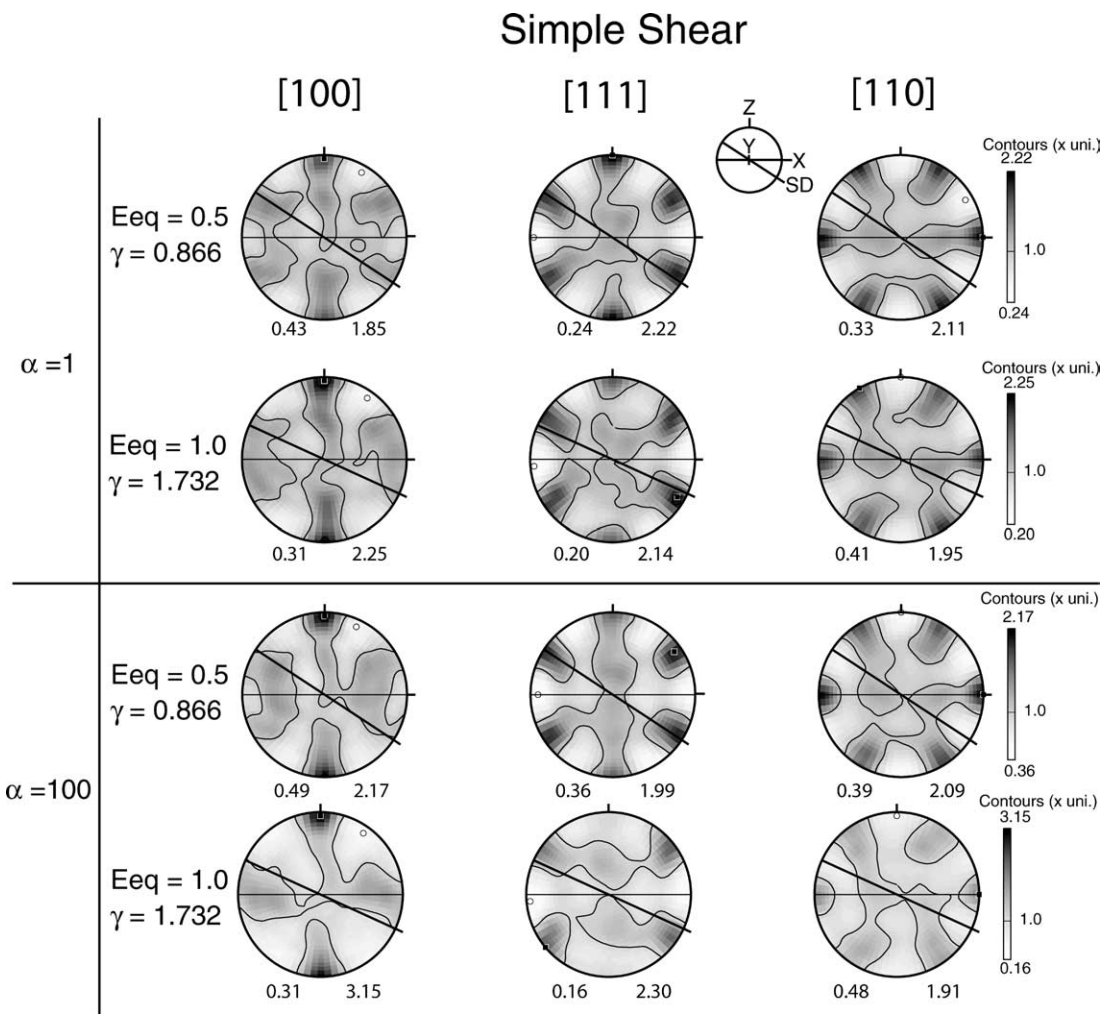

Fig. 7. Garnet [100], ⟨111⟩ and [110] pole figures for VPSC models $\alpha = 1$ and $\alpha = 100$ and equivalent strains of 0.5 ($\gamma = 0.866$) and 1.0 ($\gamma = 1.732$) for simple shear. *X* and *Z* are finite strain axes with *X* and *Z* being the direction of maximum and minimum extension directions, respectively. A horizontal line marks the *XY* finite strain plane. SD is the shear direction in the shear plane (marked by inclined line). Lower hemisphere plots. The contour at one times multiple of a uniform distribution is plotted. An inverse log grey scale also displays densities.

strains of 0.5 and 1.0 are shown in Fig. 5. The [100], [111] and [110] pole figures show the characteristic symmetry of axial compression with a relatively strong alignment of [100] and [111] parallel to the compression axis and weaker alignment of [110] normal to the compression axis. With increasing strain, the degree of preferred orientation increases. At higher strain ($E_{eq} = 1$) the difference between the $\alpha = 1$ and $\alpha = 100$ models becomes clear, in particular in the [111] pole figures. For $\alpha = 1$, [111] displays a point maximum parallel to the compression axis, whereas for $\alpha = 100$, it is the [100] axes that display the strongest concentration. In both models, the highest concentration of [100] is always parallel to the compression axis. The pole figure densities for [100] and [111] may reach high values of over five multiples of a uniform distribution (mud).

For pure shear deformation, the difference between low and high strain and between $\alpha = 1$ and 100 are less marked (Fig. 6). The overall intensities of the pole figures are much lower than in axial compression with values never exceeding 4 mud. There is a relatively strong alignment of [100] and [111] parallel to the compression axis and an alignment of [110] parallel to the extension axis. Again, as in axial compression, for $E_{eq} = 1$ and $\alpha = 1$, [111] has a point maximum parallel to the compression axis, whereas for $\alpha = 100$ [100] axes display the strongest concentration.

For simple shear, probably the most relevant strain regime for geological studies, we have a systematic alignment of the ⟨111⟩ axes with the shear direction (SD) and the ⟨110⟩ with the shear plane normal (SPN) (Fig. 7). Again the difference between the $\alpha = 1$ and $\alpha = 100$ models is only evident at the higher strain ($\gamma = 1.73$). As in the other deformation modes, the differences are more pronounced in [100] and [111] pole figures, both having a tendency to display two maxima in the $\alpha = 100$ models, rather than the three maxima observed in the $\alpha = 1$ models. The strong alignment of [100] with the main shortening direction (*Z*) is still a major feature in the simple shear mode; however, [111] axes are rather aligned with shear

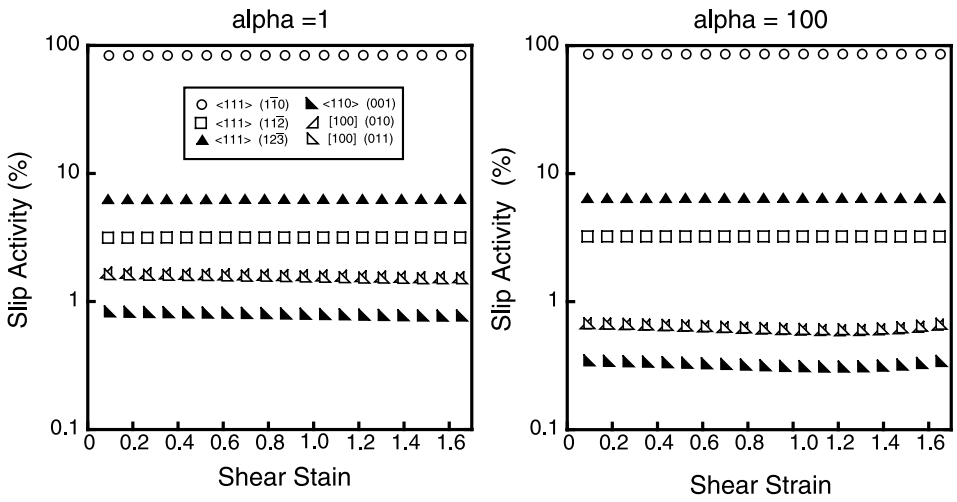

Fig. 8. Garnet slip system activities for VPSC models $\alpha = 1$ and $\alpha = 100$ for simple shear as a function of shear strain. The slip system activity is given as a percentage of the total activity on a log scale.

direction. As in axial compression and pure shear modes there is a concentration of [110] axes parallel to the extension axis (X) in simple shear. Although the preferred orientation patterns are quite characteristic, pole figure densities are never very high in simple shear, with 3.15 mud being the maximum density. In contrast with observations and simulations for simple shear deformation of low-symmetry minerals, such as olivine and quartz, in the present simulations we do not observe a progressive rotation of the dominant slip system towards parallelism with the macroscopic shear reference frame. Increasing shear strain does not significantly modify the CPO (neither patterns nor intensity) for strains higher than 0.5. We interpret this behaviour as resulting from the large number of slip systems available in the garnet cubic structure.

Analysis of the simulations for these three deformation modes also allow us to infer the CPO evolution in response to combinations of pure and simple shear, such as transpression or transtension. In transpression, shortening normal to the shear plane leads to extension normal to the shear direction. We expect, therefore, CPO intermediate between the axial compression and simple shear ones, with some dispersion of all three axes with the normal to the shear plane as the zone axis. In transtension, extension normal to the shear plane will probably induce a slight anti-synthetic rotation of the CPO to maintain the parallelism of the [110] axes with the maximum stretching direction (X).

The question of which glide systems are contributing to the CPO development can be illustrated by a plot of the evolution of the activity of the various slip systems with increasing strain for $\alpha = 1$ and $\alpha = 100$ models in simple shear (Fig. 8). The ⟨111⟩ glide direction dominates with slip on (110) planes accounting for over 86% of activity; this activity is constant with increasing shear strain. The [100] glide direction only contributes about 3% and the ⟨110⟩(001) system represents less than 1% of the total slip activity. The slip system activities are almost identical for axial compression and pure shear.

4. Crystal preferred orientation in naturally deformed garnets

Garnet CPO in a series of naturally deformed eclogites was recently measured by electron back-scattered diffraction (EBSD) technique as part of a study on the deformation and seismic properties of high-pressure rocks (Bascou et al., 2001; Bascou, 2002). These samples are representative of various geometries and intensities of deformation under eclogitic metamorphic conditions. The CPO of the major component, omphacite clinopyroxene, as well as a detailed presentation of the geological setting of each sample have been already reported by Bascou et al. (2001). In the present study we focus on the CPO of garnet. Peak pressure and temperature conditions experienced by each sample, compositions, as well as the EBSD measurement procedure are presented in Table 1.

Most samples have experienced pressures over 2.1 GPa (Table 1). Temperatures recorded by the samples of Alpe Arami (Dobrzhinetskaya et al., 2002) and Gourma (Caby, 1994) are rather high (>700 °C). Except for the Alpe Arami sample, eclogite from the Alps are rather low-temperature. Temperatures for the Monviso, Mt. Mucrone and Siviez-Mischabel eclogites range from 570 to 680 °C. Still lower temperatures were obtained for the Western Gneiss Region eclogites (480–580 °C; Labrousse, 2001). Intermediate temperatures and pressures (670 ± 50 °C at a minimum of pressure of 1.46 GPa) were estimated for the three eclogite samples from a shear zone on the island of Holsnøy in the Bergen Arc, Norway (Boundy et al., 1992).

These rocks have a volume fraction of garnet between 20 and 40%, so in general the garnet does not form the load-bearing framework, which is composed of plastically

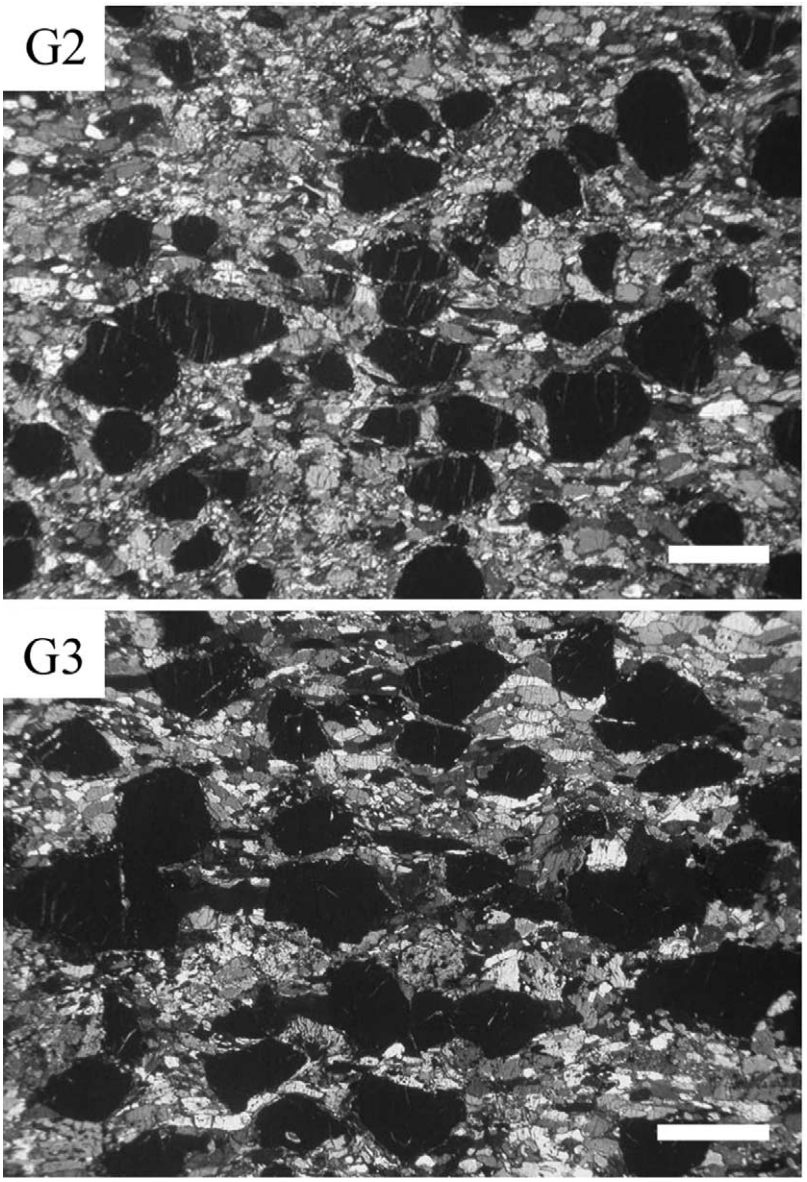

Fig. 9. Photomicrographs of eclogite from the Hundskeften Shear Zone on Holsnoy Island. Samples of series G represent an eclogitic rim around a granulitic boudin. Omphacite and garnet are the major mineral phases and phengite, zoisite and kyanite occur as minor phases. Lineation is defined by the shape preferred-orientation of omphacite and a mineralogical layering of omphacite-rich and omphacite-poor, garnet-rich layers mark foliation. Photomicrograph of garnet rich area on *XZ* plane, polarized light. Scale bar = 2 mm.

Table 1
P, *T* conditions of eclogitic metamorphism, analytical data, volume fraction of garnet and omphacite, and grain size for the studied samples

Sample location (sample)	*P* (GPA), *T* (°C) peak	Mean ref.	EBSD procedure	Step (μm)	Grt (%)	Omph (%)	Mean grain size (μm)
Alpe Arami (AB.E)	>2.1, >750	[1]	Manual	*y*: 1000	30	60	omph: 4000 × 1000; grt: 800
Mt. Mucrone (eclo 01)	1.3–1.6, 600–650	[2]	Automatic	*x*,*y*: 500	25	55	omph: 3000 × 1000 (porph); <1000 (recr); grt: 1000
Monviso (γ 4129)	>2.4, 570–670	[3]	Manual	*y*: 500	20	65	omph: 2000 × 500 (porph); <40 (recr); grt: 500 × 300
Siviez-Mischabel (γ 3638)	>1.5, 620–680	[4]	Automatic	*x*,*y*: 500	20	65	omph: 500 × 200; matrix < 300; grt: 500
Bergen Arc (G3)	>1.5, 620–720	[5]	Automatic	*x*,*y*: 400	25	65	omph: 500 × 200; grt: 1500 × 1000
Nordfjord (WGR) (B6)	>2.1, 480-580	[6]	Manual		35	55	omph: 3000 × 1000; grt: 2000
Gourma (S522)	>2.7, 700–750	[7]	Manual	*y*: 1000	25	70	omph: 1500 × 800 and 400 × 200; grt < 1000

Omph: omphacite; grt: garnet; porph: porphyroclasts; recr: recrystallized grains. [1] Dobrzhinetskaya et al. (2002); [2] Lardeaux et al. (1982); [3] Messiga et al. (1999); [4] Thélin et al. (1990); [5] Boundy et al. (1992); [6] Labrousse (2001); [7] Caby (1994).

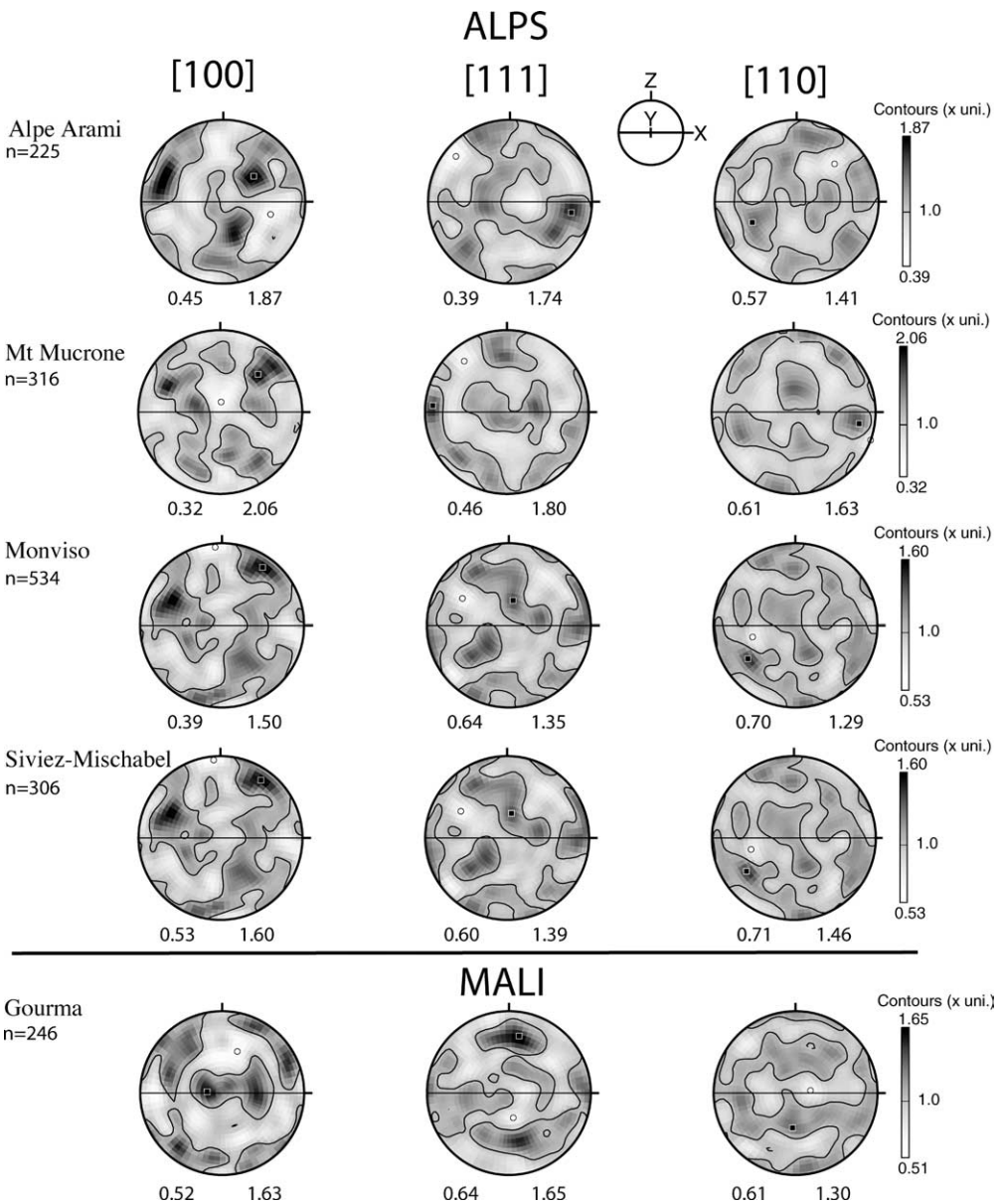

Fig. 10. Garnet [100], ⟨111⟩ and [110] pole figures from naturally deformed samples from the Alps and Mali. *X* and *Z* are mineral lineation and foliation, respectively. Lower hemisphere plots. The contour at one times multiple of a uniform distribution is plotted. An inverse log grey scale also displays concentrations. Minimum and maximum for density each pole figure is given. (*n*) gives the number of individual crystal measurements for each sample.

deformed omphacite. Indeed all samples display strong omphacite CPO (Bascou et al., 2001). Analysis of these CPO in the light of VPSC simulations suggests that omphacite CPO in most samples is coherent with a simple shear flow accommodated by dominant glide on {110}[001], {110}⟨1$\bar{1}$0⟩, and (100)[001] systems (Bascou et al., 2002). However, the omphacite CPO of Gourma eclogite S522 is better reproduced by transpression models.

Garnet CPO is presented in the traditional structural frame characterized by the mineral lineation (*X*) and the foliation normal (*Z*), with *Y* being perpendicular to *X* and *Z*. The lineation is defined by elongated grains of omphacite and the foliation by a mineral layering marked by alternance of omphacite- and garnet-rich layers. Garnet grain sizes are in the millimetre range and they are generally rounded. However, in some samples, such as in G2 and G3, garnet may be elongated and can form almost pure layers (Fig. 9).

The CPO of garnet in these samples is never very strong (Figs. 10 and 11). Only two samples display pole figure densities over 2 mud: samples G2 and G3 from the Bergen Arc (Fig. 11). These samples are also the only ones to have a CPO pattern that resembles VPSC simulations for simple shear. Thus, only these two samples warrant further comparison with the CPO simulated for simple shear. In Fig. 12 we have contoured the pole figures of the simple shear simulations and samples G2 and G3 in exactly the same way. The pole figures of G3 have a similar pattern to the simulations, but it is by no means a perfect match. It is

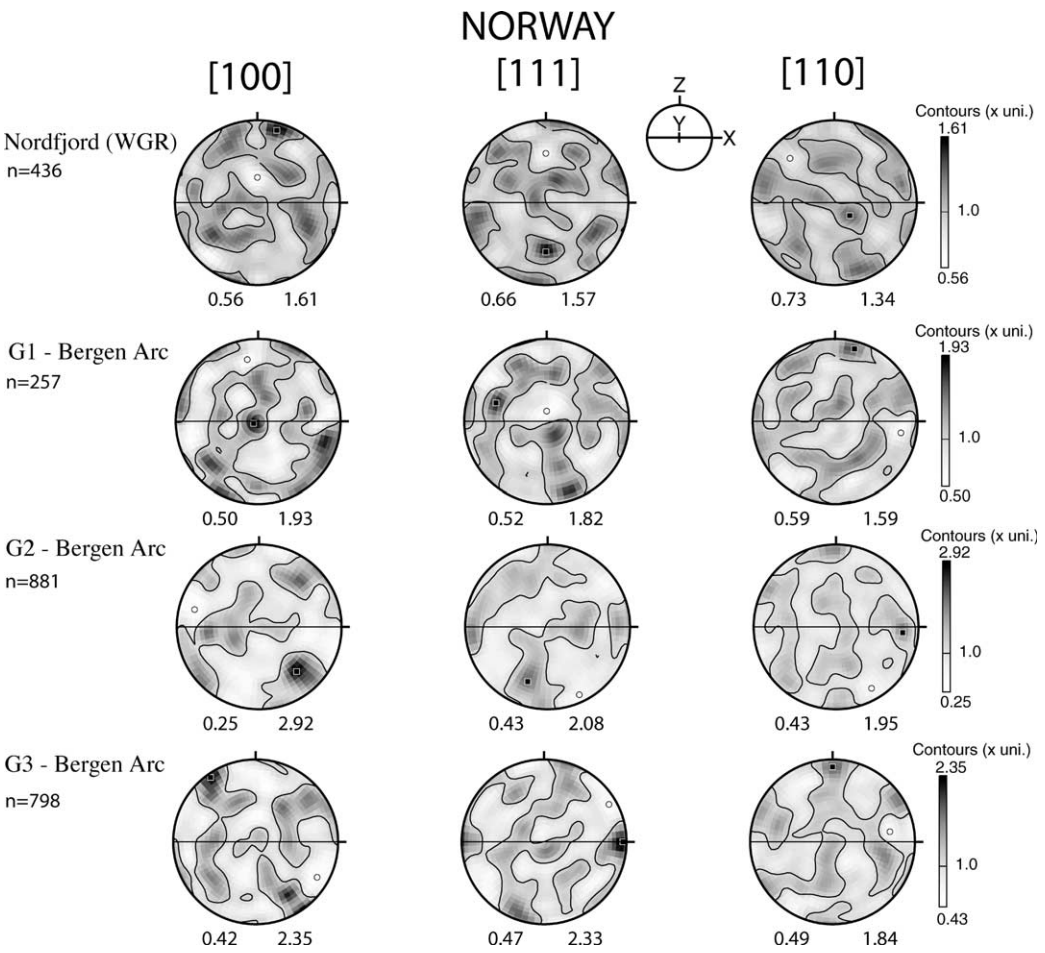

Fig. 11. Garnet [100], ⟨111⟩ and [110] pole figures form naturally deformed samples from the Norway. *X* and *Z* are mineral lineation and foliation, respectively. Lower hemisphere plots. The contour at one times multiple of a uniform distribution is plotted. An inverse log grey scale also represents concentrations. Minimum and maximum for density each pole figure is given. (*n*) gives the number of individual crystal measurements for each sample.

even difficult to say which VPSC model, $\alpha = 1$ or $\alpha = 100$, is more similar to G2 and G3.

The relative strengths of CPO of the garnet and omphacite have been evaluated by calculating the texture index *J*, which is defined as:

$$J = \int f(\mathbf{g})^2 \mathrm{d}\mathbf{g} \tag{6}$$

where $f(\mathbf{g})$ is the texture function, $\mathbf{g}$ is orientation defined by a triplet of Euler angles, for example $\mathbf{g} = (\varphi 1\ \phi\ \varphi 2)$ used by Bunge (1982) and $\mathrm{d}\mathbf{g} = 1/8\pi^2 \sin\phi\, \mathrm{d}\varphi 1\, \mathrm{d}\phi\, \mathrm{d}\varphi 2$ is the volume of the region of integration in orientation space. The *J* index has a value of one for a random distribution and a value of infinity for a single crystal. The *J* index, also known as F2, was calculated using the BearTex texture analysis package (Wenk et al., 1998). In Fig. 13 you can see that for most samples there is no correlation between the omphacite CPOs of variable strength and uniformly weak garnet CPO. However, the samples from the Bergen Arc, Norway (G1, G2 and G3) do show that as the CPO strength of garnet increases the corresponding omphacite decreases. Although this correlation may not have any statistical validity, it is interesting to note that G2 and G3 were the only samples from the nine studied that have CPOs similar to VPSC model predictions for garnet plasticity.

5. Discussion

We have made a series of VPSC simulations for silicate garnet using the slip systems identified by TEM. Comparison with CPO of garnet from naturally deformed eclogites with simulations show that only the simple shear models reproduce some of the characteristics of the naturally deformed garnet CPO. One of the main characteristics of the simple shear simulations is that the pole figures for [100], ⟨111⟩ and [110] have relatively low densities; this at least matches our naturally deformed samples. Weak garnet CPOs were also observed by Kleinschodt and co-workers (2000, 2002) and Ji et al. (2003). The clear symmetric pole figures of the VPSC simulations are not reproduced in any of the reported pole figures for naturally deformed samples, our examples G2 and G3 being perhaps the most symmetric.

Why are the pole figure densities so low? Although 66

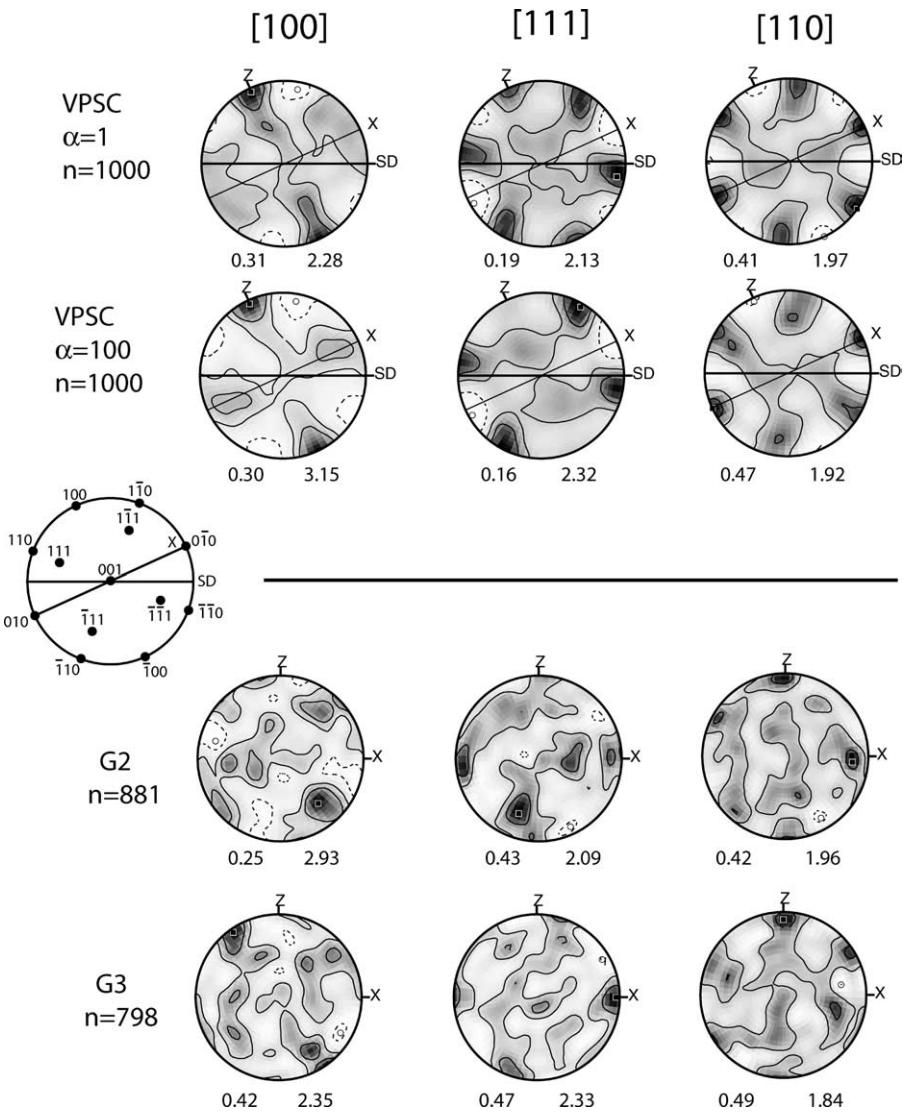

Fig. 12. Pole figures [100], ⟨111⟩ and [110] form VPSC models $\alpha = 1$ and $\alpha = 100$ for an equivalent strain of1.0 ($\gamma = 1.732$) for simple shear and naturally deformed garnet from the Bergen Arc, Norway (G2 and G3). *X* and *Z* are mineral lineation and foliation, respectively. Lower hemisphere plots. Contours are given at 0.5,1.0 and 1.5 times multiples of a uniform distribution. An inverse log grey scale also displays densities. Minimum and maximum for density each pole figure is given. (*n*) gives the number of individual crystal measurements for each sample.

slip systems are available for garnet, the 12 ⟨111⟩{110} slip systems provide over 86% of the total strain (Fig. 8). The exceptional multiplicity of slip systems in silicate garnet is certainly a factor that explains why strong preferred orientations are not produced in the simulations. Other factors affecting naturally deformed samples are the presence of other mechanically weaker minerals, for example, omphacite and quartz in eclogites. Strain is mainly accommodated by these weaker phases and garnets are only deformed to low strains. However, this strain-partitioning mechanism is not operative in the simulations. Another factor is the possible activation of other deformation mechanisms in garnet, such as diffusion creep (Wang and Ji, 2000), which will not contribute to CPO development, but will allow the garnet crystals to deform; again this possibility is not introduced in the simulations.

Why are the pole figure symmetries so poorly defined? At least two naturally deformed samples (G2 and G3) have pole figure densities similar to the simulations, but the symmetry of the pole figures are poorly defined. The fact that the naturally deformed samples are not 100% garnet would seem the most likely cause. However, simulations of 70% olivine and 30% enstatite polycrystals by Wenk et al. (1991) did not show a particularly weak enstatite CPO compared with 100% enstatite polycrystal. If the deformation mode were not ideal simple shear, this would also affect the pole figure symmetry. The magnitude of finite strain will also affect the development of the pole figure symmetry. If the initial state is a random CPO, then a certain level of finite plastic strain is necessary for recognizable pole figure symmetry to develop. It is notable that the only samples to show any correlation between the CPO strength

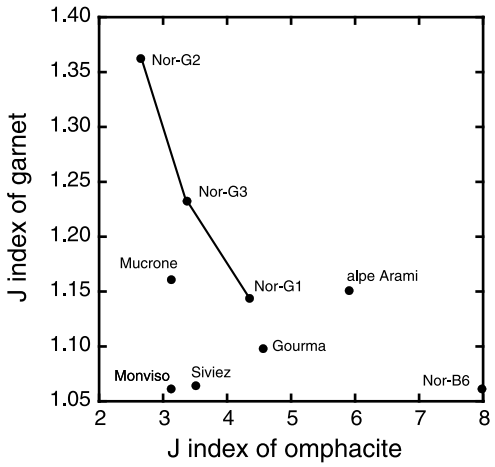

Fig. 13. Plot of the texture *J* index for garnet (vertical axis) and omphacite (horizontal axis) for all samples. Note all garnet fabrics have very low values of the texture index. Only samples G1–G3 from the same eclogite pod in the Bergen Arc (Norway) show a correlation between garnet and omphacite *J* index values.

of garnet and omphacite were the same samples (G2 and G3) that showed some similarity to the VPSC models. If the correlation between CPO strength of different minerals were confirmed by future studies, it would suggest that significant statistical mechanical interaction could occur between different mineral populations in rocks undergoing plastic deformation.

Previous interpretation of pole figures of naturally deformed garnets in terms of slip systems has relied on the use of single crystal projections (Kleinschodt and McGrew, 2000; Kleinschodt and Duyster, 2002). None of the maxima in the pole figures generated by simulations for [100], ⟨111⟩ and [110] have the same symmetry distribution or angular relationships as they would if they represented a single crystal; this is particularly apparent for ⟨111⟩ and [110].

6. Conclusions

We have simulated the CPO development of silicate garnet in axial compression, pure shear and simple shear using slip systems observed by TEM in experimentally and naturally deformed garnet. The1/2⟨111⟩{110}, 1/2⟨111⟩{112}, 1/2⟨111⟩{123}, [110]{001}, [100]{010} and [100]{011} provide 66 possible slip systems for plastic deformation of garnet. Pole figure densities for [100], ⟨111⟩ and [110] and inverse pole figures for the principal finite strain directions are in general rather low, being highest for axial compression and lowest for simple shear. Pole figures for each deformation mode had characteristic symmetries, with the [100] axis being strongly aligned with the main shortening direction, particularly at high strains in all deformation modes. As intuitively expected, in simple shear the principle glide direction ⟨111⟩ tends to align with shear direction and principle glide plan {110} with the shear plane normal. The 1/2⟨111⟩{110} system accounted for over 86% of the strain in all three deformation modes studied here.

From the naturally deformed garnets from eclogites, only the G2 and G3 samples from an intensely deformed eclogite pod from the Bergen Arc, Norway, display garnet CPO similar to those obtained in VPSC simulations for simple shear. It would seem that high temperature and high shear strain are required to produce CPOs characteristic of plastic deformation in garnet. The modest volume fractions of garnet (20–40%) in eclogites relative to more ductile minerals such as omphacite are not favourable for the accumulation of the high plastic strain necessary for development of a CPO of the relatively strong garnets. However, favourable conditions to development of garnet CPOs may exist in very high temperature granulitic domains in the lower continental crust and, more commonly, in the mantle transition zone where garnet is a volumetrically important phase. At transition zone depths, the garnet fraction may attain 40% in a pyrolite mantle and 90% in subducted MORB material.

Acknowledgements

Christophe Nevado made our excellent thin sections for EBSD. The authors thank Loïc Labrousse and Renaud Caby for discussions and providing samples. DM thanks Gilles Canova and Ricardo Lebensohn for access to the VPSC code. A. McGrew and R. Kleinschrodt are thanked for their constructive reviews. Financial support was received from the Centre National de la Recherche Scientifique (Program 'INSU-Intérieur de la Terre, Exhumation des roches profondes'). Crystal orientation measurements were made with Laboratoire de Tectonophysique EBSD/SEM system funded by grants from CNRS/INSU, Université Montpellier II, ISTEEM and NSF #EAR-9526840 'Anatomy of an Archean craton'.

References

Allen, F.M., Smith, B.K., Busek, P.R., 1987. Direct observation of dissociated dislocations in garnet. Science 238, 1695–1697.

Ando, J., Fujino, K., Takeshita, T., 1993. Dislocation microstructures in naturally deformed silicate garnets. Physics of the Earth Planetary Interiors 80, 105–116.

Bascou, J., 2002. Relations entre microstructures, mécanismes de déformation et propriétés physiques anisotropes des roches de haut grade de métamorphisme: Étude de quelques éclogites et granulites. Unpublished PhD thesis, Universidade de São Paulo & Université de Montpellier II.

Bascou, J., Barruol, G., Vauchez, A., Mainprice, D., Egydio-Silva, M., 2001. EBSD-measured lattice preferred orientations and seismic properties of eclogites. Tectonophysics 342, 61–80.

Bascou, J., Tommasi, A., Mainprice, D., 2002. Plastic deformation and development of clinopyroxene lattice preferred orientations in eclogites. Journal of Structural Geology 24, 1357–1368.

Blumenthal, W.R., Phillips, D.S., 1996. High-temperature deformation of single-crystal ytrium–aluminum garnet (YAG). Journal of the American Ceramics Society 79, 1047–1052.

Boundy, T.M., Fountain, D.M., Austrheim, H., 1992. Structural development and petrofabrics of eclogite facies shear zones, Bergen Arcs, western Norway: implications for the deep crustal deformation processes. Journal of Metamorphic Geology 10, 127–146.

Bunge, H.J., 1982. Texture Analysis in Materials Science, Butterworths, London, 599pp.

Caby, R., 1994. Precambrian coesite from northern Mali: first record and implications for plate tectonics in the trans-Saharan segment of the Pan-African belt. European Journal of Mineralogy 6, 235–244.

Carstens, H., 1969. Dislocation structures in pyropes from Norwegian and Czech garnet peridotites. Contributions to Mineralogy and Petrology 24, 348–353.

Carstens, H., 1971. Plastic stress relaxation around solid inclusions in pyrope. Contributions to Mineralogy and Petrology 32, 289–294.

Castelnau, O., Duval, P., Lebensohn, R.A., Canova, G.R., 1996. Viscoplastic modelling of texture development in polycrystalline ice with a self-consistent approach: comparison with bound estimates. Journal of Geophysical Research 101, 13851–13868.

Chen, J., Wang, Q.C., Zhai, M.G., Ye, K., 1996. Plastic deformation of garnet in eclogite. Science China Series D 39(1), 18–25.

Cordier, P., Raterron, P., Wang, Y., 1996. TEM investigation of dislocation microstructure of experimentally deformed silicate garnet. Physics of the Earth Planetary Interiors 97, 121–131.

Corman, G.S., 1993. Creep of ytrium aluminium garnet single crystals. Journal of Materials Science Letters 12, 379–382.

Dalziel, I.W., Bailey, S.W., 1968. Deformed garnets in a mylonitic rock from the Grenville front and their tectonic significance. American Journal of Science 266, 542–562.

Den Brok, B., Kruhl, J., 1996. Ductility of garnet as an indicator of extremely high temperature deformation: discussion. Journal of Structural Geology 18, 1369–1373.

Dobrzhinetskaya, L.F., Schweinehage, R., Massonne, H.-J., Green, H.W., 2002. Silica precipitates in omphacite from eclogite at Alpe Arami, Switzerland: evidence of deep subduction. Journal of Metamorphic Geology 20, 481–492.

Doukhan, N., Sautter, V., Doukhan, J.C., 1994. Ultradeep, ultramafic mantle xenoliths—transmission electron microscopy preliminary results. Physics of the Earth Planetary Interiors 82, 195–207.

Garem, H., 1983. Dissociation des dislocations et plasticité de l'oxyde de structure grenat $Gd_3Ga_5O_{12}$. PhD thesis, University of Poitiers.

Garem, H., Rabier, J., Veyssière, P., 1982. Slip systems in gadolinium gallium garnet single crystals. Journal of Material Science 17, 878–884.

Garem, H., Rabier, J., Kirby, S.H., 1985. Plasticity at crack tips in $Gd_3Ga_5O_{12}$ garnet single crystals deformed at temperatures below 950 °C. Philosophical Magazine A 51, 485–497.

Hardiman, B., Bucksch, R., Korczak, P., 1972. Observation of dislocations and inclusions in neodynium-doped yttrium aluminium garnet by transmission electron microscopy. Philosophical Magazine A 27, 777–784.

Hull, D., Bacon, D.J., 1995. Introduction to Dislocations, Butterworth-Heinemann.

Ingrin, J., Madon, M., 1995. TEM observations of several spinel-garnet assemblies: toward the rheology of the transition zone. Terra Nova 7, 509–515.

Ji, S., Martignole, J., 1994. Ductility of garnet as an indicator of extremely high temperature deformation. Journal of Structural Geology 16, 985–996.

Ji, S., Martignole, J., 1996. Ductility of garnet as an indicator of extremely high temperature deformation: reply. Journal of Structural Geology 18, 1375–1379.

Ji, S., Saruwatari, K., Mainprice, D., Wirth, R., Xu, Z., Xia, B., 2003. Microstructures, petrofabrics and seismic properties of ultra high-pressure eclogites from Sulu region, China: implications for rheology of subducted continental crust and origin of mantle reflections. Tectonophysics 370, 49–76.

Jin, Z.M., Zhang, J., Green, H.W. II, 2001. Jin, S., Eclogite rheology: implications for subducted lithosphere. Geology 29, 667–670.

Karato, S., Wang, Z., Fujino, K., 1994. High-temperature creep of yttrium–aluminium garnet single crystals. Journal of Materials Sciences 29, 6458–6462.

Karato, S., Wang, Z., Liu, B., Fujino, K., 1995. Plastic deformation of garnets: systematics and implications for the rheology of the mantle transition zone. Earth and Planetary Science Letters 130, 13–30.

Kleinschodt, R., McGrew, A.J., 2000. Garnet plasticity in the lower continental crust: implications for deformation mechanisms based on microstructures and SEM electron channeling pattern analysis. Journal of Structural Geology 22, 795–809.

Kleinschodt, R., Duyster, J.P., 2002. Deformation of garnet: an EBSD study on granulites from Sri Lanka, India and the Ivrea Zone. Journal of Structural Geology 24, 1829–1844.

Labrousse, L., 2001. L'exhumation des roches métamorphiques de très haute pression. Unpublished PhD thesis, Université de Paris 6, 314pp.

Lardeaux, J.M., Gosso, G., Kienast, J.R., Lombardo, B., 1982. Relations entre le métamorphisme et la déformation dans la zone de Sesia-Lanzo (Alpes occidentales) et le problème de l'éclogitisation de la croûte continentale. Bulletin de la Société géologique de France 24, 793–800.

Lebensohn, R.A., Tomé, C.N., 1993. A self-consistent anisotropic approach for the simulation of plastic deformation and texture development of polycrystals: application to zirconium alloys. Acta Metall. Mater. 41, 2611–2624.

Messiga, B., Kienast, J.R., Rebay, G., Riccardi, M.P., Tribuzzio, R., 1999. Cr-rich magneslochloritoid eclogites from the Monviso ophiolites (Western Alps, Italy). Journal of Metamorphic Geology 17, 287–299.

Molinari, A., Canova, G.R., Azhy, S., 1987. A self-consistent approach of the large deformation crystal polycrystal viscoplasticity. Acta Metallurgica 35, 2983–2994.

Parthasarathy, T.A., Mah, T., Keller, K., 1992. Creep mechanism of polycrystalline yttrium aluminum garnet. Journal of the American Ceramics Society 75, 1756–1759.

Poirier, J.P., 1985. Creep of Crystals, Cambridge University Press, Cambridge.

Prior, D.J., Wheeler, J., Brenker, F.E., Harte, B., Matthews, M., 2000. Crystal plasticity of natural garnet: new microstructural evidence. Geology 28, 1003–1006.

Prior, D.J., Wheeler, J., Peruzzo, L., Spiess, R., Storey, C., 2002. Some garnet microstructures: an illustration of the potential of orientation maps and misorientation analysis in microstructural studies. Journal of Structural Geology 24, 999–1001.

Rabier, J., 1979. Dissociation des dislocations dans les oxydes de structure grenat. Application à l'étude de la déformation plastique du grenat de fer et d'yttrium (YIG). Thèse de Doctorat d'Etat, Université de Poitiers.

Rabier, J., Garem, H., Veyssière, P., 1976a. Transmission electron microscopy determinations of dislocation Burgers vectors in plastically deformed yttrium iron garnet single crystals. Journal of Applied Physics 47, 4755–4758.

Rabier, J., Veyssière, P., Grilhé, J., 1976b. Possibility of stacking faults and dissociation of dislocations in the garnet structure. Phys. Stat. Sol. (a) 35, 259–268.

Rabier, J., Veyssière, P., Garem, H., Grilhé, J., 1979. Sub-grain boundaries and dissociations of dislocations in yttrium iron garnet deformed at high temperatures. Philosophical Magazine A 39, 693–708.

Rabier, J., Veyssière, P., Garem, H., 1981. Dissociation of dislocation with $a/2\langle 111\rangle$ Burgers vectors in YIG single crystals deformed at high temperature. Philosophical Magazine A 44, 1363–1373.

Ross, J.V., 1973. Mylonitic rocks and flattened garnets in the southern Okanagan of British Columbia. Canadian Journal of Earth Sciences 10, 1–17.

Taylor, G.I., 1938. Plastic strain in metals. Journal of the Institute of Metals 62, 307–324.

Taylor, G.I., Elam, C.F., 1926. The distortion of iron crystals. Proceedings of the Royal Society of London A112, 337–361.

Thélin, P., Sartori, M., Lengeler, R, Schaerer, J.P., 1990. Eclogites of Paleozoic or early Alpine age in the basement of the Penninic Sivlez-Mischabel nappe, Wallis, Switzerland. Lithos 25, 71–88.

Tommasi, A., Mainprice, D., Canova, G., Chastel, Y., 2000. Viscoplastic self-consistent and equilibrium-based modeling of olivine lattice preferred orientations: implications for the upper mantle seismic anisotropy. Journal of Geophysical Research 105, 7893–7908.

Voegelé,V., 1998. Etude par microscopie électronique en transmission de la plasticité des grenats. Unpublished Ph.D. thesis, Université des Sciences et Technologie de Lille.

Voegelé, V., Ando, J.I., Cordier, P., Liebermann, R.C., 1998a. Plastic deformation of silicate garnet. I. High pressure experiments. Physics of the Earth and Planetary Interiors 108, 305–318.

Voegelé, V., Cordier, P., Sautter, V., Sharp, T.G., Lardeaux, J.M., Marques, F.O., 1998b. Plastic deformation of silicate garnets. II. Deformation microstructures in natural samples. Physics of the Earth and Planetary Interiors 108, 319–338.

Voegelé, V., Liu, B., Cordier, P., Wang, Z., Takei, H., Pan, P., Karato, S.I., 1999. High temperature creep in a 2–3–4 garnet: $Ca_3Ge_2Ge_3O_{12}$. Journal of Materials Science 34, 4783–4791.

Wang, Z., Ji, S., 1999. Deformation of silicate garnets: brittle ductile transition and its geological implications. The Canadian Mineralogist 37, 525–541.

Wang, Z., Ji, S., 2000. Diffusion creep of fined-grained garnetite: implications for the flow strength of subducting slabs. Geophysical Research Letters 27, 2333–2336.

Wang, Z., Karato, S., Fujino, K., 1996. High temperature creep of single crystal gadolinium gallium garnet. Physics and Chemistry of Minerals 23, 73–80.

Wenk, H.-R., Bennett, K., Canova, G.R., Molinari, A., 1991. Modelling plastic deformation of peridotite with the self-consistent theory. Journal of Geophysical Research 96, 8337–8349.

Wenk, H.-R., Matthies, S., Donovan, J., Chateigner, D., 1998. Beartex: a window-based program system for quantatitive texture analysis. Journal of Applied Crystallography 31, 262–269.